A compact optical system design for underwater fishing lamp

MINJU FAN, YUNCUI ZHANG[*], XUFEN XIE, YUANG CHEN, DA PAN, SHUHAN YAN
Graduate School, Dalian Polytechnic University Dalian 116034, China

With the development of deep-sea lighting technology, it is necessary to design lighting systems to solve the problems of rapid light attenuation for different lighting purposes. This paper presents a compact optical system which combines a central lens and a surrounding lens through closely connected free-form surface to achieve two modes of lighting, long distance and wide-angle range. In the design example, an optical system of 3×3 square LED array is constructed with the combined lenses, which has long-distance lighting 100 m in ocean water and 120 ° large lighting angle simultaneously. The lighting system with small volume, compact structure and multiple functions can be realized and adapted to submarine lighting applications.

1. Introduction

Underwater detection, identification, fishing and other fields are in great need of illumination optical systems. The lighting effect of underwater luminaires is greatly affected because of the attenuation of water on light [1]. With the development of optical technology, LED lighting performance source luminaries with novel lighting performance are gradually replacing the traditional fluorescent lamps [2-3].

LED has the advantages of long life, high luminous efficiency, good color rendering, low carbon and environmental protection. Improving the performance of LED underwater lighting is an important problem in the research of optical system [4]. ADI Susanto et al. studied the difference in the visual effects of LED lamps and fluorescent lamps underwater. They pointed out that the attenuation effect varies according to different seawater quality and light source. Compared with fluorescent lamp, LED light source has higher efficiency in underwater fishing for its spectral characteristics [5]. Fang Ming Chung *et al.* presented the underwater light intensity distribution by establishing the underwater LED light transmission model and analyzed the illumination and the lighting area under different emission angles, which can be used as the basis for the design and research of underwater LED lamp [6]. Hu Bo et al. proposed a theoretical model for the distribution of spectral irradiance with distance on the main optical axis of underwater light sources, which was expected to be used for modeling underwater light fields and laying the theoretical foundation for the subsequent design of underwater fishing lights [7]. Wang

Kai et al. investigated the conditions under which large-view LED arrays produce uniform illumination through Monte Carlo ray-tracing simulations, and found that the uniformity increases abnormally with the increase of specific LED spacing [8]. Shen et al. designed a non-axisymmetric lens by plotting light intensity distribution curves in the horizontal and vertical planes to obtain an illumination area with alternating light and dark distribution, which can effectively attract fish around fishing boats. And using Fourier series and energy mapping methods to obtain multiple concentric circles of the illumination surface, it was found that fish were more adapted to congregate in dark areas, which proved that the illumination pattern is effective for gathering fish [9-10]. Lai Min Feng et al. designed and optimized a multi segment free-form surface lens, which had high lamp performance, and the efficiency was three times that of the traditional lamps [11]. Tsung-Xian Lee et al. added a dual-wavelength LED to the original white LED, which would perform spectrum compensation at each illumination distance to restore its good light quality. The result showed that such a dynamic light source can successfully maintain correlated color temperature at 6000 K and color rendering index above 80 under different underwater illumination distances [12]. Kuo et al. used the light tracing method to design a concentrating optical lens, which had an optimized light distribution, the ability to concentrate light as well as the ability to increase irradiance in the illuminated area, without affecting the amount of capture while fuel consumption can be saved by 20.2% [13]. Nguyen et al. applied the Gaussian decomposition method to the free-form lens design, and

when the proposed LED fishing/working lamp was used instead of the HID fishing lamp, an illumination efficiency of 91% could be achieved with only one-third of the power consumption, so the method could meet the lighting needs for both fishing and boat activities [14].

In the above research, it was found that the attenuation of light by sea water affected the transmission distance and range of light. Freeform lenses always are applied in the optical design to solve the problems to improve the illuminance performance of the lamps in the sea water. In this paper, a compact and flexible lighting optical system is produced to meet the underwater fishing requirements.

2. Underwater light field analysis

The dissolved substances, suspended bodies and a wide variety of active organisms contained in seawater cause various inhomogeneities in seawater, making the energy attenuation of light transmission in water more severe than in the atmosphere [15]. The transmission distance of light in the air is farther, because the air density is smaller, its absorption and scattering effect of light is also relatively small. The density of seawater is greater than the density of air, which has a strong absorption and scattering effect on light.

When light propagates in seawater, the water molecules and particles in seawater have an absorption effect on light, converting the energy of light into heat energy and making the energy of the light beam attenuate. Seawater absorption of light in different spectral regions is different, the strongest absorption of ultraviolet and infrared wavelengths, the highest absorption of visible wavelengths, respectively, red and yellow wavelengths. The absorption of the blue and green wavelengths is relatively small, with the least attenuation of blue light at wavelengths from 450 to 475 nm.

When light propagates in seawater, water molecules in water and suspended particles in water also produce a strong scattering effect on light, and this scattering is divided into two types: forward scattering and backward scattering. Forward scattering refers to the light propagation in seawater, when the photons encounter the suspended particles in the water produced forward scattering. Backward scattering is the backward scattering that occurs when light propagates in water and encounters suspended particles in the water. In light scattering in seawater, the scattered photons do not disappear, but their propagation paths are altered. As a result of multiple scattering, some photons scattered from the main beam can still return to the main beam, so the scattering effect in seawater is stronger the higher the intensity of the incident light [16].

Affected by the absorption and scattering effect of seawater on light, the propagation of light in seawater is according to the exponential law of decay. Formula (1) defines the Lambert-Beer underwater transfer model for traditional light sources.

$$I_l = I_0 e^{-\alpha l} \tag{1}$$

where I_l represents the light intensity of the laser beam after passing through the water with thickness of l and I_0 is the incident light intensity. The attenuation coefficient $\alpha(\lambda)$ is composed of two parts

$$\alpha(\lambda) = a(\lambda) + b(\lambda) \tag{2}$$

Among them $a(\lambda)$ is the absorption coefficient of the water. The absorption properties of the material components contained in the seawater determine the seawater absorption properties, and the magnitude of the absorption coefficient depends on the wavelength. $b(\lambda)$ represents the scattering coefficient of the water body. In the scattering of seawater, molecular scattering is basically constant and accounts for only a small part of the total attenuation of light transmission, and the scattering characteristics depend mainly on the composition and number of suspended particles in seawater.
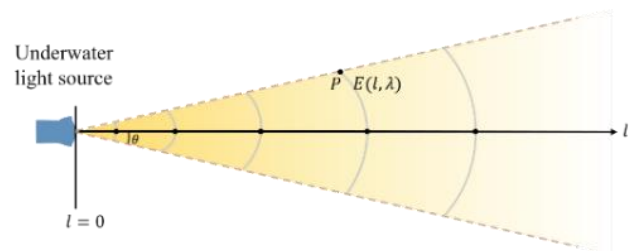

Fig. 1. Schematic diagram of underwater optical transmission (color online)

The schematic diagram of underwater light transmission is shown in Fig. 1. The light emitted by the underwater light source is transmitted in the water, λ represents the light wavelength, θ is the angle between the direction of emission and the normal of the surface source. When the emission distance is l, it can get the irradiance of point P on the target plane as $E(l, \lambda)$.

Based on the above analysis, in terms of the effect of underwater light attenuation, the intensity of the spectral radiation decreases with transmission distance. The fast light attenuation rate in the deep sea makes the lighting system have the problems of short lighting distance and narrow irradiation range.

2.1. Attenuation Characteristics of Different Water Bodies

The attenuation coefficient of light in coastal water and ocean water are very different due to the diverse contents of suspended particles and plankton. The transmission characteristics are related with the kind of sea

water [17]. Ocean water and coastal water are two typical marine environments, and other seawater properties are usually between them. Therefore, the performance of ocean water and coastal water is studied and analyzed in this paper. The light attenuation coefficient diagram of these two kinds of seawater is shown in Fig. 2.
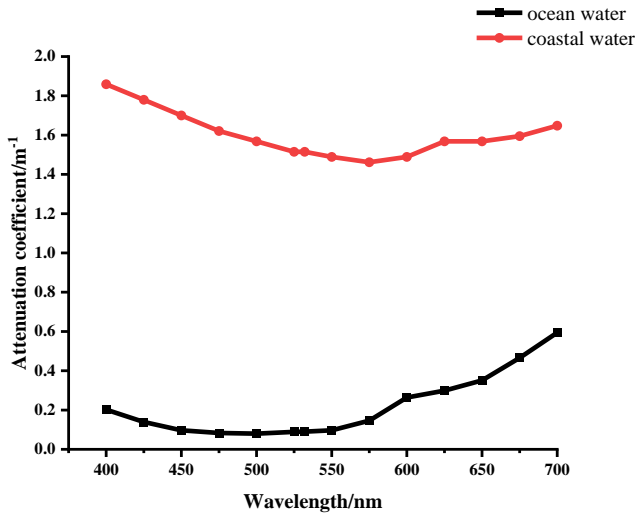

Fig. 2. Light attenuation coefficient of different water quality (color online)

When the light is transmitted in the water, the light intensity at different distances in space is directly related to the attenuation coefficient of the water. According to the different attenuation performance of light, this paper selects two typical seawater. The attenuation of light by the two seawater follows formula (1), and the following light intensity attenuation curves can be obtained.
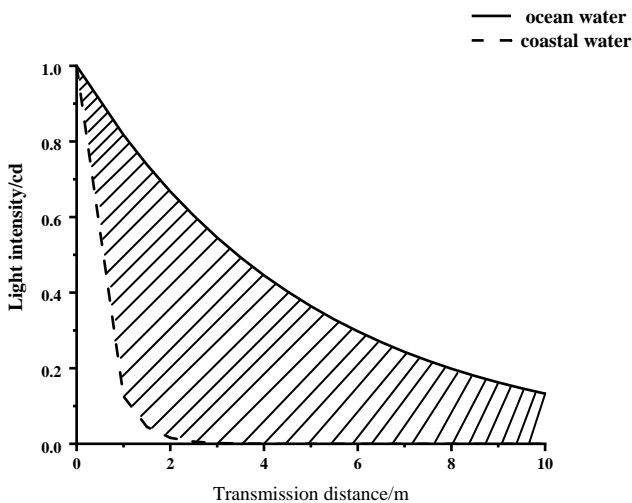

Fig. 3. Light intensity attenuation curves of coastal water and ocean water

It can be seen from the figure that with the increase in distance, in the state of coastal water and ocean water, the spectral intensity of coastal water decreases rapidly, while the attenuation of ocean water is relatively slow. Generally, the attenuation characteristics of seawater are between the above two typical seawater, and the light intensity attenuation characteristics of light are in the shaded part in the figure.

Taking the light distribution characteristics of the Lambert light source emitted by LED light source as an example, the light transmission characteristics in deep-sea lighting are studied. The radiant characteristic of the light source is a Lambert type, and the brightness of the Lambert radiator does not vary with the angle θ. The spatial light intensity distribution function of the Lambertian LED light source is as follows:

$$I_\theta = I_0 \cos\theta \qquad (3)$$

where I_θ is the luminous intensity of the spatial angle θ, I_0 is the central luminous intensity.

The light attenuation of the LED light source in seawater is determined by the transmission distance and the light emission angle. So the relationship between the transmission distance l and the central transmission distance l_0 in the direction of the divergence angle θ is expressed by the following equation.

$$l = \frac{l_0}{\cos\theta} \qquad (4)$$

According to the formulas (1) (3) (4), the LED light source at the divergence angle θ, the light intensity I at the transmission distance l and the initial light intensity I_0 of the central light can be obtained as shown in formula (5):

$$I = I_0 \cos\theta \, e^{-\alpha\frac{l_0}{\cos\theta}} \qquad (5)$$

According to this formula, we can calculate that the wavelength of light at 500 nm changes from -90° to 90°. In ocean water, the relative light intensity distributions at different transmission distances are shown in Fig. 4, and it can be seen that the light intensity distribution patterns are different at 1 m, 3 m, 5 m, 7 m and 10 m transmission distances. The light decays more rapidly in the offshore, giving the relative light intensity distribution curves at distances of 1 m, 2 m, etc. The relative light intensity decreases fast in the coastal water, and the curves of it at 0.5 m, 1 m, 1.5 m, 2 m and 2.5 m are shown in Fig. 4.
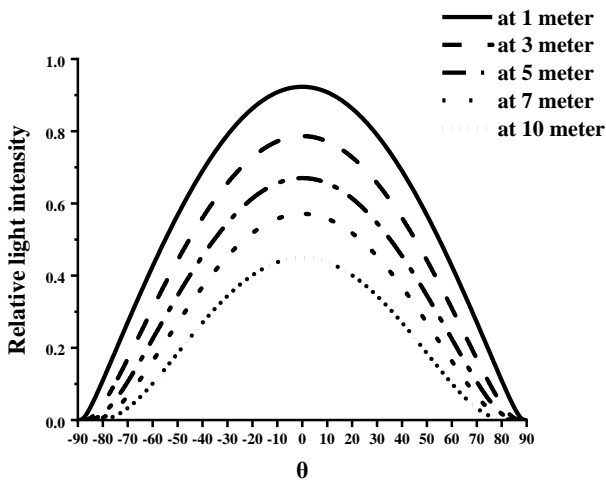
Fig. 4. Variation of light intensity in ocean water at different distances
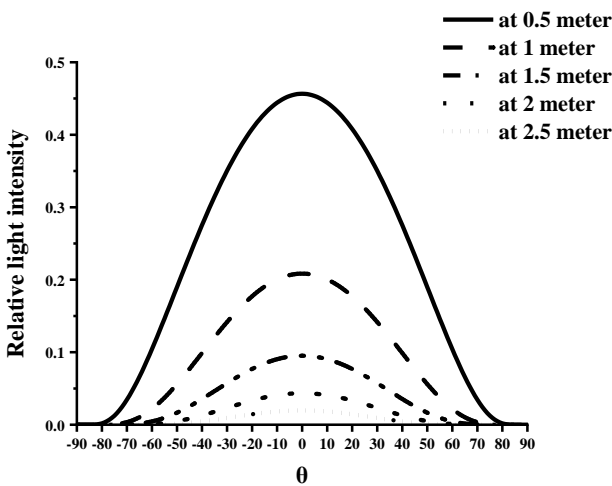

Fig. 5. Variation of light intensity in coastal water at different distances

It can be seen from the figures that the attenuation rate of light is non-linear depending on the spatial transmission angle, that is, the effect of different transmission distances on the light intensity is related to the transmission angle. These phenomena have led to the impact of attenuation due to different spatial transmission distances and transmission angles into consideration for lighting design in seawater.

3. Design of the underwater compact optical system

When lighting underwater, large-scale lighting is required when searching for fish, and long-distance lighting in specific areas is required after determining the direction. Two kinds of lenses are needed to achieve such

different lighting requirements. The goal of this design is to make the structural design reasonable and compact. This paper proposes an optical system design method that combines two lenses compactly to produce long-distance collimated light and large-angle illumination.

3.1. Design of Lamps

The underwater optical lighting system designed in this paper needs to be divided into two parts, the middle part uses TIR collimating lens to convert the light of LED into a collimating beam, and the surrounding uses large angle beam for illuminating the underwater environment. The schematic diagram of underwater light is shown in Fig. 6.
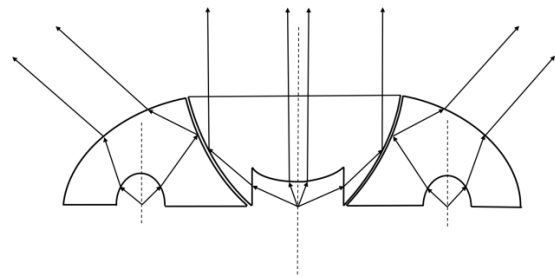

Fig. 6. Schematic diagram of illumination lamp

In this paper, a collimating TIR lens is used in the center of the optical unit to illuminate long distance object. The design of TIR collimating part is shown in Fig. 7.
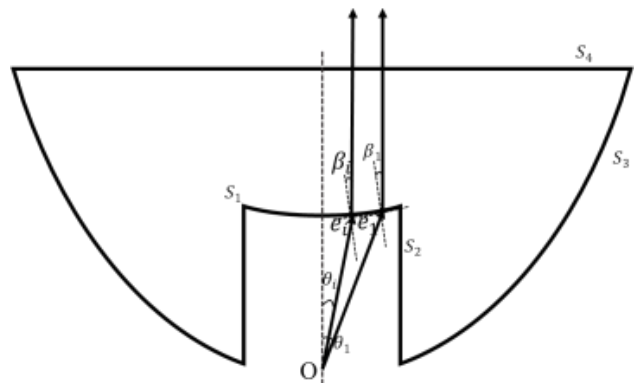

Fig. 7. Light path diagram of TIR collimation part

The light is emitted from the point O, and the angle between the light and the optical axis is θ_1, θ_2, ... θ_i, the intersection of these rays and free-form surface S_1 is e_1, e_2,..., e_i, the coordinate of each point on free-form surface S_1 is $e_i(x_i, y_i)$, after S_1 refraction, the angle between the light and the optical axis is $\beta_1, \beta_2, ... , \beta_i$, constructing S_1 surface is the process of obtaining the

coordinates of a series of points e_1, e_2, …, e_i.

The sampled light rays emitted from the light source O are sampled at equal angular intervals, Oe_i exits in a direction parallel to the Y axis after passing through S_1 surface, so according to the law of refraction:

$$\sin(\beta_i + \theta_i) = n \sin \beta_i \qquad (6)$$

In the formula, β_i is the angle between the light O emitted from the surface S_1 and the normal vector passing through the point Oe_i, n is the refractive indices of sea water. Thus, the slope of the tangent line past point e_i can be obtained as

$$k_i = \tan \beta_i = \frac{\sin \theta_i}{n - \cos \theta_i} \qquad (7)$$

The slope of the tangent line passing through e_i can be expressed as

$$k_i = \frac{\sin \theta_i}{n - \cos \theta_i} = \frac{y_{i+1} - y_i}{x_{i+1} - x_i} \qquad (8)$$

The relationship between the abscissas of point e_{i+1} satisfies

$$x_{i+1} = y_{i+1} \tan \theta_{i+1} \qquad (9)$$

Combining formulas (8) and (9) can be obtained

$$y_{i+1} = \frac{(n - \cos \theta_i) y_i - x_i \sin \theta_i}{n - \cos \theta_i - \sin \theta_i \tan \theta_{i+1}} \qquad (10)$$

$$x_{i+1} = \frac{(n - \cos \theta_i) y_i - x_i \sin \theta_i}{n - \cos \theta_i - \sin \theta_i \tan \theta_{i+1}} \tan \theta_{i+1} \qquad (11)$$

From equations (10) and (11), it can be seen that the coordinates of point e_{i+1} can be represented by the coordinates of point e_i, and the angle Oe_i and Oe_{i+1} between the ray θ_i and θ_{i+1} and the Y axis. Therefore, once you know the coordinates of any point on the surface S_1, you can use this iterative relationship to find the coordinates of the next point. Through continuous iteration, you can find the coordinates of any point on the surface S_1.

The schematic diagram of the reflected part of the light path is shown in Fig. 8. The light in the small-angle area is output through the refraction lens, and the light with a large angle first enters the surface S_2, refracts to the surface S_3, and is reflected by the surface S_3, and finally passes through the surface S_4. Below the surface S_1 is a cylindrical cavity, which can be used to place the LED light source. As shown in the schematic diagram of the boundary conditions of the lens in Fig. 9. Here it is assumed that the angular range of the transmitted part of the light is $0 \sim \theta_1$, and the angular range of the reflected part of the light is $\theta_1 \sim P_1$, where θ_1 is the boundary angle between the refraction part and the reflection part, and P_1 is the Y axis of the bottom edge of the light OF_1. The coordinates of the point F_t of the t ray OF_t incident on the surface S_2 are shown as

$$x_{2t} = d, \quad y_{2t} = d \tan(\frac{\pi}{2} - P_t) \qquad (12)$$

In formula (12), P_t is the angle between the light OF_t emitted by the light source and the Y axis. Here d is the radius of the cylindrical cavity, $d = h \tan \alpha$ and α is the boundary angle between the refraction part and the reflection part, and h is the height of the cylindrical cavity.
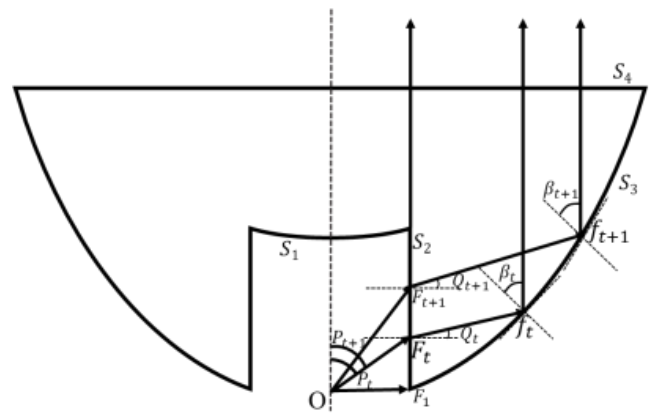

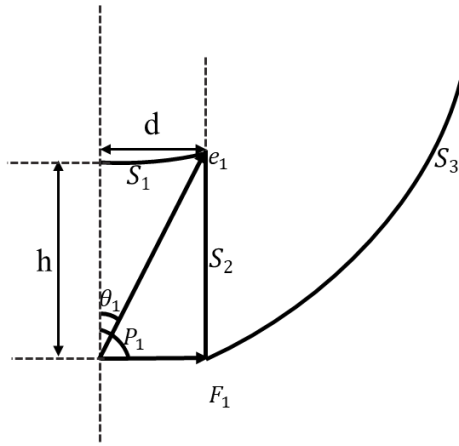*Fig. 8. Schematic diagram of the reflected part of the light path*

Fig. 9. Schematic diagram of the boundary conditions of the lens

The light incident on the cylindrical side wall will be refracted and follow the refraction law. Here the light follows Snell's law as follows:

$$\sin(\frac{\pi}{2} - P_t) = n_1 \sin Q_t \qquad (13)$$

In Formula (13), Q_t is the angle between the light $F_t f_t$ emitted from the surface S_2 and the normal vector, n_1 is the refractive index of the medium.

The light $F_t f_t$ exits in the direction parallel to the Y axis after being reflected by the surface S_3, and the reflection angle β_t is gotten according to the reflection law

$$\beta_t = \frac{Q_t + \frac{\pi}{2}}{2} \qquad (14)$$

Therefore, the slope of the tangent to the point f_t on the surface S_3 can be obtained as

$$k_t = \tan \beta_t = \tan(\frac{Q_t + \frac{\pi}{2}}{2}) = \tan(\frac{\frac{\pi}{2} + \arcsin\frac{\cos P_t}{n_1}}{2}) \quad (15)$$

Next, the iterative relationship between adjacent sampling points f_t and f_{t+1} on the surface S_3 is constructed. When the coordinates (x_{3t}, y_{3t}) of the point f_t are obtained, if the number of sampling points on the surface S_3 is relatively large, the intersection of the tangent line passing the point f_t and the t+1th sampled ray emitted from the point f_{t+1} can be approximated as

point f_{t+1}. The slope of $F_{t+1} f_{t+1}$ can be expressed as

$$m_t = \tan(Q_{t+1}) = \frac{y_{3,t+1} - y_{2,t+1}}{x_{3,t+1} - x_{2,t+1}} = \frac{y_{3,t+1} - d \tan(\frac{\pi}{2} - P_{t+1})}{x_{3,t+1} - d} \qquad (16)$$

The tangent slope passing through the point f_t can also be expressed as

$$k_t = k_t = \tan \beta_t = \tan(\frac{Q_t + \frac{\pi}{2}}{2}) = \tan(\frac{\frac{\pi}{2} + \arcsin\frac{\cos P_t}{n_1}}{2}) = \frac{y_{3,t+1} - y_{3,t}}{x_{3,t+1} - x_{3,t}} \qquad (17)$$

Combining formula (16) and formula (17) can be obtained

$$x_{3,t+1} = \frac{d \tan Q_{t+1} - d \tan(\frac{\pi}{2} - P_{t+1}) - k_t x_{3,t} + y_{3,t}}{\tan Q_{t+1} - k_t} \qquad (18)$$

$$y_{3,t+1} = \frac{dk_t \tan Q_{t+1} - dk_t \tan(\frac{\pi}{2} - P_{t+1}) - k_t x_{3,t} \tan Q_{t+1} + y_{3,t} \tan Q_{t+1}}{\tan Q_{t+1} - k_t} \qquad (19)$$

For the reflective surface S_3, the point f_1 has been given in the initial conditions. Using the above-mentioned iterative relationship between adjacent sampling points, all the sampling points on the entire reflective surface can be found.

The surrounding lens is designed to divergent the light to illuminate large scale area. The schematic diagram of surrounding lens is shown in Fig. 10.
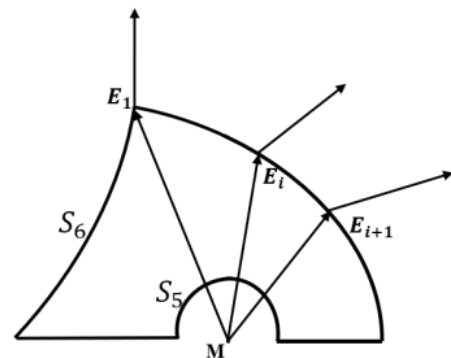

Fig. 10. Light path diagram of surrounding part of the optical unit

There are 8 LEDs inside the surrounding lens, and 8 LEDs are located at the bottom of the surrounding lens to achieve a large angle of light dispersion. The light is

emitted from point M, surface S_5 is a circular arched spherical surface, does not have any reflection refraction, so the light from the LED through the circular arched spherical surface S_5 after the direction of light does not change. Part of the light from the LED in the surrounding lens passes through the circular arched spherical surface S_5 and is directly incident to the second surface S_6 in the surrounding lens, which is reflected by the surface S_6 and then incident to the surface S_7 of the surrounding lens, which is finally emitted by the surface S_7. There is also a portion of light incident directly to the surface S_7 through the circular arching spherical surface S_5, and the light exits through the surface S7. The curvature of the face of the second surface S_6 remains the same as the curvature of the outer surface S_3 of the collimated lens. So the bus of the surface S_6 can be deduced from equations (18) and (19).
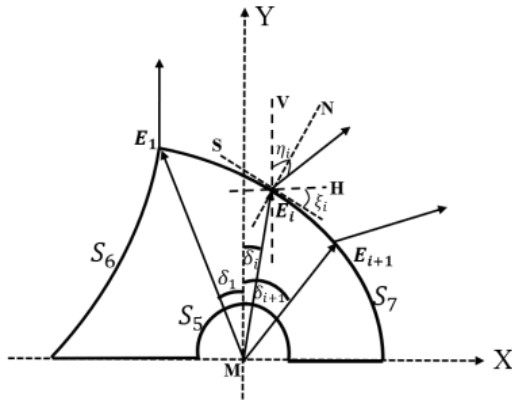

Fig. 11. Schematic diagram of the light path exiting through the S7 surface

The schematic diagram of the optical path of light exiting through the free surface S_7 is shown in Fig. 11. The angles of the rays from point M and the Y-axis are $\delta_1, \delta_2, \cdots \delta_i$. The intersection of these rays with surface S_7 is E_1, E_2,...E_i, the highest point E_1 is the highest point on surface S_6 and is also on the same level as the highest point on surface S_3, so the coordinates of E_1 can be expressed as $(x_{3,\max} + j, y_{3,\max})$, where j denotes the interval between surface S_6 and surface S_3. The vectors **N**, **S**, **V** and **H** are the normal, tangent and perpendicular and horizontal lines of the surface S_7 where the point E_i is located, and the angle between the refracted ray and the perpendicular of the surface S_7 are $\eta_1, \eta_2, \cdots \eta_i$. The angle between the horizontal line and the tangent line is $\xi_1, \xi_2, \cdots \xi_i$. According to the law of refraction the vector form has

$$1 + n^2 - 2n(\mathbf{Out} \bullet \mathbf{In})^{1/2} \bullet \mathbf{N} = \mathbf{Out} - \mathbf{In} \bullet n \qquad (20)$$

In which n is the refractive index of the lens, **Out** is the unit vector of the incident light, and **In** is the unit vector of the incident light. From this, the normal vector $\mathbf{N_i}$ can be obtained, and then the unit vector $\mathbf{S_i}$ of the vector **S** is related to $\mathbf{N_i}$ as

$$\mathbf{N_i} \bullet \mathbf{S_i} = 0 \qquad (21)$$

The slope of the tangent line of the ray passing through the point E_i on the surface S_7 can be obtained from the vector **S** as

$$k_{E_i} = \tan \xi_i \qquad (22)$$

Here the line $E_i E_{i+1}$ coincides with the tangent line of the point E_i to the surface S_7, so the relationship between the point $E_{i+1}(x_{i+1}, y_{i+1})$ and the point $E_i(x_i, y_i)$ is

$$k_{E_i} = \tan \xi_i = \frac{y_{E_{i+1}} - y_{E_i}}{x_{E_{i+1}} - x_{E_i}} \qquad (23)$$

Furthermore, the equation of the line ME_{i+1} is

$$x_{E_{i+1}} = y_{E_{i+1}} \tan \alpha_{E_{i+1}} \qquad (24)$$

The iterative relationship between the coordinates of two adjacent sampling points can be obtained after combining equations (23) (24) as follows.

$$x_{E_{i+1}} = \frac{\tan \alpha_{i+1}(y_{E_i} + x_{E_i} \tan \xi_i)}{1 + \tan \alpha_{i+1} \tan \xi_i} \qquad (25)$$

$$y_{E_{i+1}} = \frac{y_{E_i} + x_{E_i} \tan \xi_i}{1 + \tan \alpha_{i+1} \tan \xi_i} \qquad (26)$$

For the initial point coordinates of surface S_7 are $E_1(x_{3,\max} + j, y_{3,\max})$ given, so starting from the initial value, the coordinates of the next point can be found by using this iterative relation of equation (23)(24), and the coordinates of any point on surface S_7 can be found by continuous iteration, so that the complete bus of surface S_7 can be found.

3.2. Optical performance analysis

The center of the optical system model uses a TIR collimating lens to achieve long-distance collimated lighting, and 8 large-angle light sources around it can achieve large-angle lighting, thereby expanding the lighting range and improving fishing efficiency.

The compact optical unit has two functions of

collimation and large angle lighting. The LED light source is chosen as XLamp XP-G3 Royal Blue, which has a good waterproof design and can maintain security in water. The physical diagram of XLamp XP-G3 Royal Blue is shown in Fig. 12.

XLamp XP-G3 Royal Blue is a laser light source with the wavelength of 451 nm, which satisfies the requirement of low absorption by seawater. Its luminous flux is 911 *lm* and the maximum power is 6 W. In the design of this paper, one light source is set in the center light source to collimate the light, and eight light sources are set around it to achieve large-scale lighting. According to the relevant parameters of XLamp XP-G3 Royal Blue, the optical characteristics parameters of the designed single underwater fishing light can be obtained as shown in Table 1.

Fig. 12. Physical picture of XLamp XP-*G3 Royal Blue*

Table 1. LED optical characteristic parameter table

Light source parameters / Light source selection	Number	Power /W	Luminous flux /lm	Center wavelength /nm
Central light source	1	6	911	451
Surrounding light source	8	48	7288	451

Through the above design method and process, the final design of a single fishing light optical system model diagram is shown in Fig. 13.
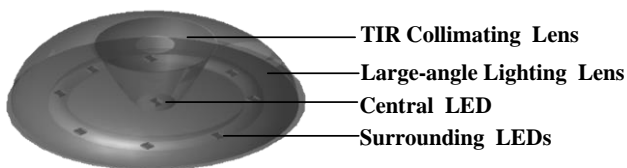

Fig. 13. Model diagram of illumination lamp optical unit

The total power of central and surrounding light source is 6W and 48W respectively. The surrounding light source are eight LEDs with power of 48 W. The total luminous flux of the two light sources is 911 *lm* and 7288 *lm* respectively. The light simulation results of the central and surrounding light sources in deep-sea water are shown in Fig. 14.
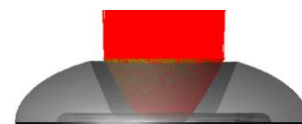
(a)

(b)

Fig. 14. Lighting simulation of (a) central light source and (b) surrounding light sources (color online)

The central lens can collimate the LED light, and the light energy is relatively concentrated, which can carry out long-distance transmission. The light of the surrounding light source passes through the divergent lens for large-scale illumination. The light intensity distribution curves of these two light sources are shown in Fig. 15.
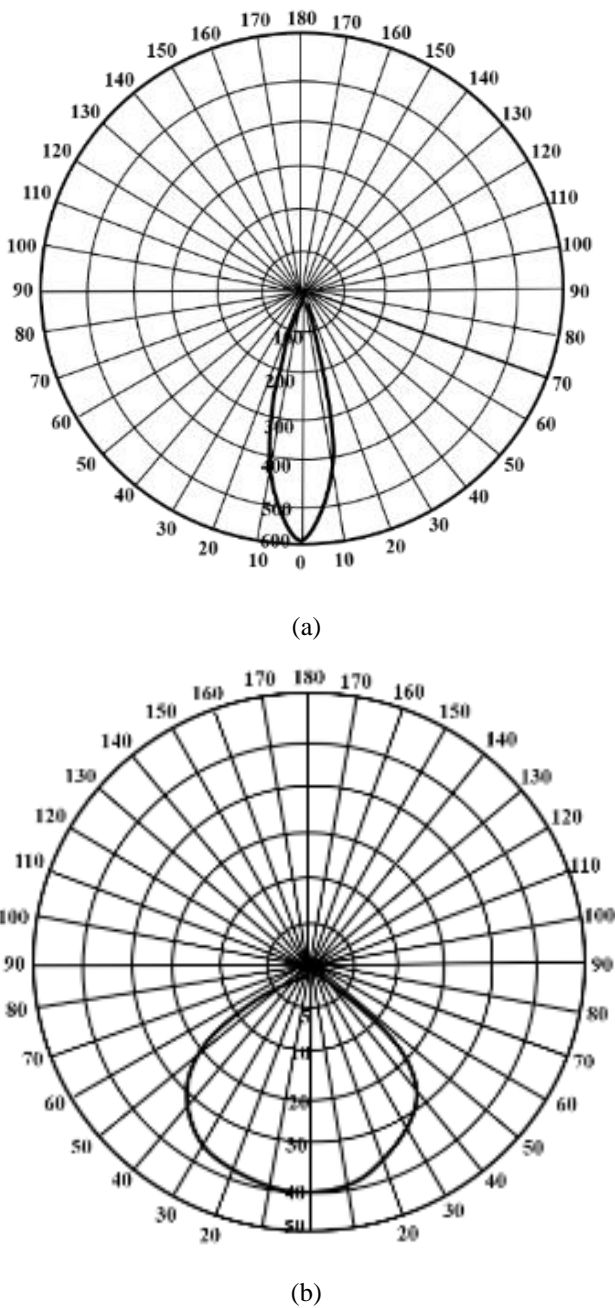
(a)

(b)

Fig. 15. Light intensity distribution of (a) central and (b) surrounding light source

As an integrated chip light source, the beam angle of the central light source after passing through the collimating lens is 20°. The surrounding light is refracted from the PMMA material into the water, and the beam angle is 120°. Two kinds of light distribution are suitable for different needs of deep-sea lighting. In deep-sea fishing, the central light source can be used for fish detection, and the surrounding light source can be used for fish attraction.
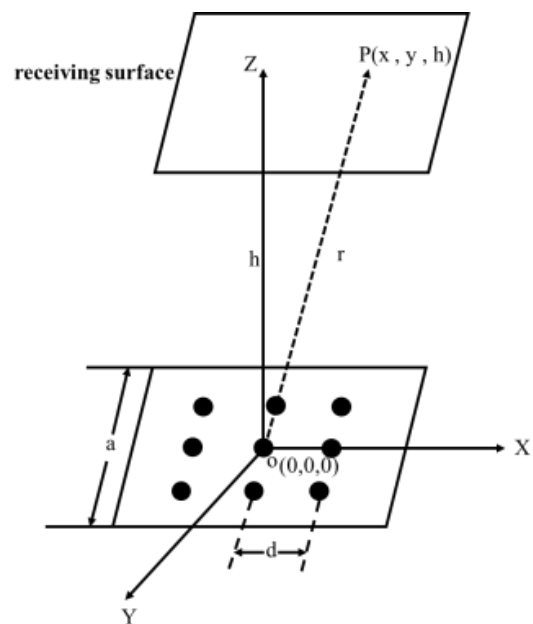
4. Design and performance analysis of unit array

Based on the above optical lens, the compact optical system of illumination lamp is designed by a 3×3 single surface array design method. The lens array of 3 realizes lighting in specific direction and meets the requirements of lighting distance and lighting range by array. The design diagram of LED array is shown in Fig. 16.

Fig. 16. Design diagram of LED array

4.1. LED array theory and model

In order to meet the needs of high-power deep-sea lighting, the performance of array lighting is analyzed. The LED light sources designed above are spatially arranged according to a certain law, and the overall lighting effect are affected by the arrangement of light sources.

In the spatial arrangement, the lenses are arranged on a plane. The schematic diagram of the square LED array is shown in Fig. 17. The square LED array has M LED chips uniformly distributed in each row and each column, that is, the total number of LED chips in the square LED array is $N=M\times M$, the square array is in the z=0 plane, and the chip coordinates of the center of the square array are at (0,0,0). The target plane z=h.

Fig. 17. The diagram of LED square array

If an LED chip is set at point $(X,Y,0)$ and the coordination of the illumination point P is $(x,\ y,\ h)$, the illumination E and intensity I satisfy the cosine law.

$$E(\ x,\ y,\ h) = \frac{I_0 \cos\theta}{r^2} \qquad (27)$$

In equation (27), r is the distance from the LED to point P, h is the vertical distance. But due to underwater light attenuation, resulting in illumination E energy loss, so combined with the underwater light attenuation formula (1), the illumination of a single LED chip at point P is

$$E(x,y,h) = \frac{I_0 e^{-\alpha\frac{l_0}{\cos\theta}}\cos\theta}{r^2} = \frac{I_0 e^{-\alpha\frac{l_0}{\cos\theta}}h}{[(x-X)^2+(y-Y)^2+h^2]^{\frac{3}{2}}} \qquad (28)$$

If there are n LED chips on the plane where z = 0, the illumination at point P is

$$E(x,y,h) = \sum_{n=1}^{n} \frac{I_0 e^{-\alpha\frac{l_0}{\cos\theta}}h}{[(x-X_i)^2+(y-Y_i)^2+h^2]^{\frac{3}{2}}} \qquad (29)$$

In equation (29), $(X_i, Y_i, 0)$ is the coordinate of the ith LED in a square array, in which the distance between two adjacent LED is d. According to equation (29), the illuminance of P point on the target plane of the square LED array is as follows:

$$E(x,y,h) = \sum_{j=\frac{-(M-1)}{2}}^{\frac{(M-1)}{2}} \sum_{j=\frac{-(M-1)}{2}}^{\frac{(M-1)}{2}} \frac{I_0 e^{-\alpha\frac{l_0}{\cos\theta}}h}{[(x-jd)^2+(y-jd)^2+h^2]^{\frac{3}{2}}} \qquad (30)$$

The illumination generated in space is related to the distance between LEDs and the transmission distance. The calculation method can be used to analyze the spatial illumination of the surrounding light sources.

4.2. Design results and analysis

In order to achieve lighting in all directions, the designed lamps are installed with 3×3 optical unit array on each light-emitting surface. Among them, there are 9 LEDs as central light sources for long-distance lighting, with a total power of 54W. 72 LEDs with power of 432W are used as the surrounding light sources for large-scale lighting. The optical system parameters and light utilizations of the lamp on a surface are shown in Table 2.

Table 2. Performance parameters of lighting system

parameters / Light source	Power /W	Luminous flux /lm	Received luminous flux /lm	Light utilization
Central light source	54	8199	6623.3	80.8%
Surrounding light source	432	65592	39387	60.1%

It can be seen from the table that the light utilization rate of the surrounding light sources is significantly lower than that of the center light source when the light is just emitted. This may be due to the large light divergence angle of the surrounding light sources, causing some of the light to reflect in the lens for many times and cannot be emitted effectively and some of the light becomes stray light and cannot irradiate the target area.

The luminous surface of the lamp can produce two kinds of lighting effects, which can be selected according to different application needs. There are two kinds of lighting effects: the central light source with concentrated light intensity and high intensity, and the surrounding light source with scattered light intensity and low intensity. The illumination distribution of two modes produced by the light emitting surface of the lamp at 1m is shown in the Fig. 18.
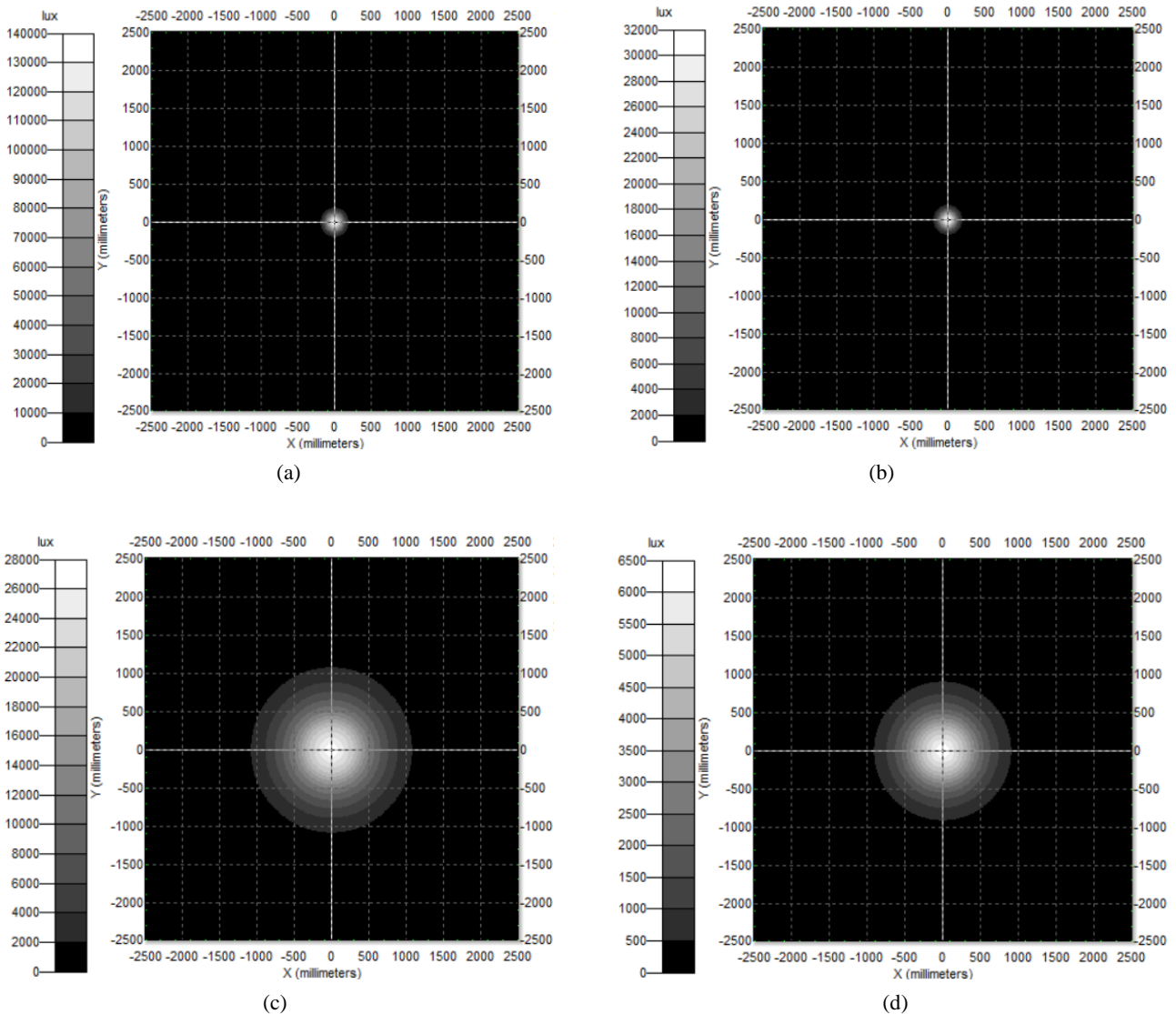
Fig. 18. The illuminance diagram of the central light sources in ocean water (a) and coastal water (b) and surrounding light sources in ocean water (c) and coastal water (d)

As can be seen from the figure above, the effects of the two lighting modes can be realized in this system. Light concentration is conductive to long-distance propagation for detection, and beam divergence is suitable for large-scale lighting. Due to the influence of seawater attenuation, the illumination of the central light source and surrounding light sources in the coastal water state are significantly lower than those in the ocean water state. The light intensity distribution curve is obtained at 1 m is shown in Fig. 19.

As shown in Fig. 19, the central light source has a high light intensity, which can reach a maximum light intensity of about 18000 cd in the air state, and the maximum light intensity is attenuated by 6% and 78% under the attenuation effect of ocean water and coastal water compared with that in the air state. The maximum light intensity of the surrounding light sources in the air state can reach about 15000 cd. Due to the attenuation effect of ocean water and coastal water, the maximum light intensity is attenuated by 11.9% and 80% compared with that in the air state. The attenuation of the light intensity of the central light source and the surrounding light source in coastal water is much larger than that in ocean water, which is in line with the light attenuation trend of the two types of seawater depicted in Fig. 2. The central light source beam angle is small, which can achieve long-distance illumination and detect the target. The dispersion angle of the surrounding light source either in the air, or the attenuation of the two kinds of seawater, the dispersion angle can reach 120 °, thus allowing a wide range of illumination to identify objects.
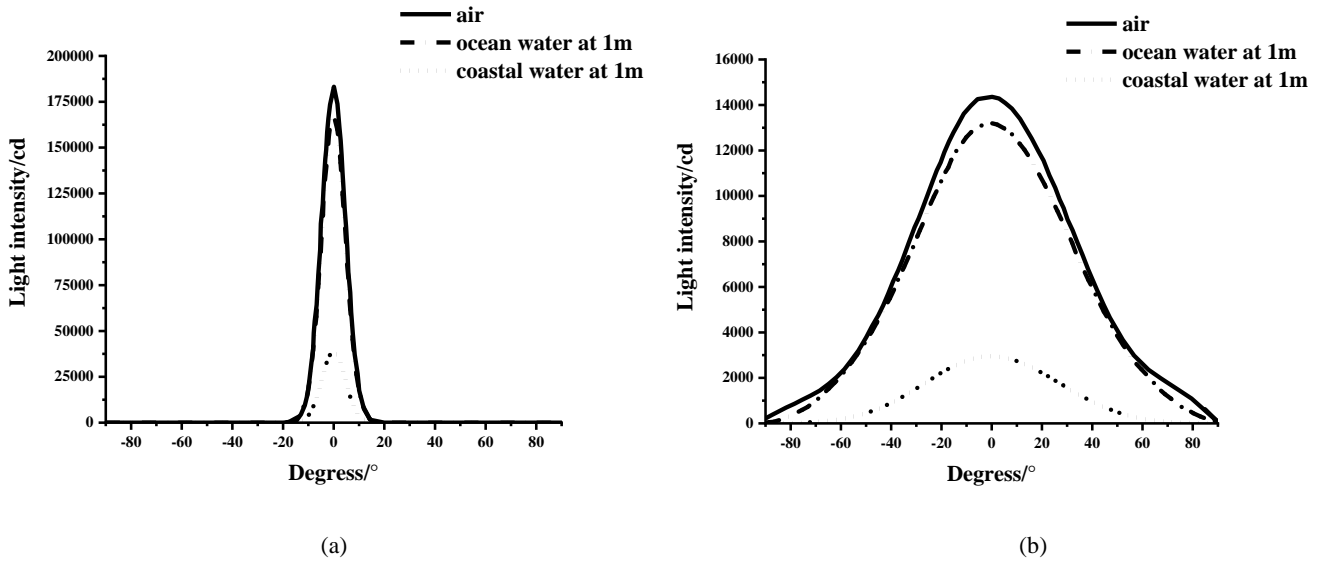
(a)

(b)

Fig. 19. The light intensity distribution curves of (a) the central light source and (b) the surrounding light source

In order to study the effective lighting distance and range of deep-sea, the fishing illuminance of several fish is given in Table 3 [18]. In general, the illumination suitable for fishing is 0.1 lux ∼ 20 lux and 10 lux is regarded as the minimum required value of illumination [19-20].

The light attenuation is serious in the sea water species, so it can only meet the detection and recognition of different species of fish within a certain distance. According to the analysis of different species of fish capture illumination, we take 10 lux as the minimum illumination. The light intensity attenuation curves of the central light source and surrounding light sources in the ocean water and coastal water are shown in Fig. 20.

Table 3. Suitable illuminance for trapping several fishes

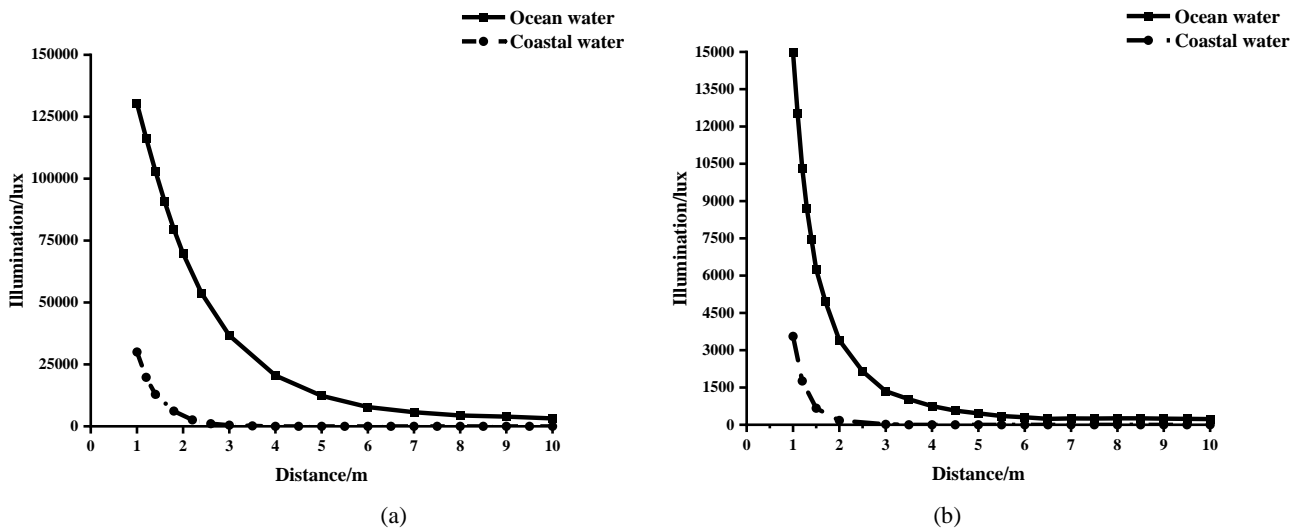| Species of fish	Trapping illuminance (lx)
Blue trevally	10^{-1}~10^{-3}
Mackerel	10^{-1}~7
Turtle	10^{-1}~18
Squid	10^{-1}

(a)

(b)

Fig. 20. The light intensity attenuation curves in different seawater of (a) central light source (b) surrounding light sources

According to the results of the simulation, for mackerel, mudfish, squid, mackerel, Japanese horse mackerel and other fish, in the case of ocean water, the central light source can be trapped 100 m, but in the case of coastal water the transmission distance can only reach 10 m. The free-form lens with uniform illumination distribution is used in the surrounding light source, so the effective transmission angle of them is 120°, and the lighting distance is decreased sharply compared with central light source in the sea.

5. Conclusion

This research uses the light attenuation characteristics of different seawaters to design a new type of compact deep-sea light. The optical system is divided into two parts: center lens and surrounding lens, which simultaneously realizes the functions of large-angle light emission and long-distance transmission. A 3×3 LED lighting array is constructed, and the illuminance and the maximum achievable emission angle of it transmitted under water are analyzed. The underwater simulation results show that the longest distance of the central light source is 100 m in ocean water and the surrounding light sources can reach 120° wide angle lighting. The system has compact structure and different lighting modes, which can adapt to the deep-sea machine vision, deep-sea fishing and other applications.

References

[1] S. C. Shen, H. J. Huang, J. C. Hsieh, H. J. Shaw, Appl. Ocean. Res. **32**(2), 137 (2010).

[2] N. Q. Anh, M. F. Lai, H. Y. Ma, H. Y. Lee, Appl. Opt. **53**(29), 140 (2014).

[3] P. Gu, X. Liu, Y. Ding, Z. Zheng, Opt. Express **16**(17), 12958 (2008).

[4] G. Wang, L. Wang, F. Li, G. Zhang, Appl. Opt. **51**(11), 1654 (2012).

[5] A. Susanto, R. Irnawati, Mustahal, M. A. Syabana, Turk. J. Fish. Aquat. Sc. **17**(2), 283 (2017).

[6] S. C. Shen, C. Y. Kuo, M. C. Fang, Int. J. Adv. Robot. Syst. **10**(3), 183 (2013).

[7] B. Hu, C. P. Zhao, Y. Yang, X. Zhang, H. Song, J .Tao, Infrared. Laser Eng. **48**(9), 299 (2019).

[8] Q. Zong, W. Kai, C. Fei, X. Luo, L. Sheng, Opt. Express **18**(16), 17460 (2010).

[9] S. C. Shen, H. J. Huang, Opt. Express **20**(24), 26135 (2012).

[10] S. C. Shen, J. S. Li, M. C. Huang, Opt. Express **22**(11), 13460 (2014).

[11] M. F. Lai, N. D. Q. Anh, J. Z. Gao, H. Y. Ma, H. Y. Lee, Appl. Opt. **54**(28), 69 (2015).

[12] T. X. Lee, Y. M. Li, J. Y. Shen, Opt. Eng. **60**, 091506 (2021).

[13] C. Y. Kuo, S. C. Shen, IEEE Access **6**, 66664 (2018).

[14] A. Nguyen, V. H. Nguyen, H. Y. Lee, Curr. Opt. Photonics **1**(3), 233 (2017).

[15] P. C. Y Chang, J. C. Flitton, K. I. Hopcraft, E. Jakeman, J. G. Walker, Appl. Opt. **42**(15), 2794 (2003).

[16] L.V. Nguyen, M. Vasiliev, K. Alameh, IEEE. Photonic. Tech. L **23**(7), 450 (2011).

[17] B. D. Tramski, Limnol. Oceanogr. **47**(3), 911 (2002).

[18] Y. Yamashita, Y. Matsushita, T. Azuno, Fish. Res. **113**(1), 182 (2012).

[19] W. G. Qian, X. J. Chen, L. Lin, J. Dalian Ocean Univ. **27**(5), 471 (2012).

[20] X. J. Chen, W. G. Qian, Y. Zheng, J. Shanghai Fish. Univ. **13**(2), 176 (2004).

_____

[*]Corresponding author: zhang_yc@dlpu.edu.cn